*atmosphere*

MDPI

*Article*

# Added Value of Aerosol-Cloud Interactions for Representing Aerosol Optical Depth in an Online Coupled Climate-Chemistry Model over Europe

**Laura Palacios-Peña [1,†], Juan P. Montávez [1,†], José M. López-Romero [1,†], Sonia Jerez [1,†], Juan J. Gómez-Navarro [1,†], Raquel Lorente-Plazas [1,†], Jesús Ruiz [1,†] and Pedro Jiménez-Guerrero [1,2,*,†]**

1 Physics of the Earth, Regional Campus of International Excellence "Campus Mare Nostrum", Campus de Espinardo, University of Murcia, 30100 Murcia, Spain; laura.palacios1@um.es (L.P.-P.); montavez@um.es (J.P.M.); jm.lopezromero@um.es (J.M.L.-R.); sonia.jerez@um.es (S.J.); jj.gomeznavarro@um.es (J.J.G.-N.); lorente.plazas@gmail.com (R.L.-P.); jrm@um.es (J.R.)

2 Biomedical Research Institute of Murcia (IMIB-Arrixaca), 30120 Murcia, Spain

* Correspondence: pedro.jimenezguerrero@um.es; Tel.: +34-868-88-8175

† These authors contributed equally to this work.

Received: 7 February 2020; Accepted: 31 March 2020; Published: 8 April 2020


**Abstract:** Aerosol-cloud interactions (ACI) represent one of the most important sources of uncertainties in climate modelling. In this sense, realistic simulations of ACI are needed for a better understanding of the complex interactions between air pollution and the climate system. This work quantifies the added value of including ACI in an online coupled climate/chemistry model (WRF-Chem, 0.44° horizontal resolution, years 2003 to 2010) in order to assess whether there is an improvement in the representation of aerosol optical depth (AOD). Modelling results for each species have been evaluated against the Copernicus Atmosphere Monitoring Service (CAMS) reanalysis, and AOD at 675 nm has been compared to AERONET data. Results indicate that the improvements of the monthly biases are around 8% for total AOD550 when including ACI, reaching 20% for the monthly bias in AOD550 coming from dust. Moreover, the temporal representation of AOD550 largely improves (increase in the Pearson time correlation coefficients), ranging from 6% to 20% depending on the chemical species considered. The benefits from this improvement overcome the problems derived from the high computational time required in ACI simulations (eight times higher with respect to simulations not including aerosol-cloud interactions).

**Keywords:** aerosol-cloud interactions; regional climate; aerosol optical depth; air quality modelling; air quality-climate interactions

## 1. Introduction

The presence of pollutants in the atmosphere, especially aerosols, impacts on the radiative balance, and modifies atmospheric conditions (temperature, precipitation, clouds, atmospheric dynamics) [1]. The modification by atmospheric aerosols of radiation and clouds (among other meteorological variables) represents a key topic when characterizing the climate of the Earth. The potential impacts of aerosol-radiation-cloud interactions may include (e.g., [2–5]): (1) exceedances of the aerosol critical levels causing changes in the patterns of extreme events; (2) high variation of levels of air pollutants; (3) changes in atmospheric dynamics, etc. Therefore, air quality problems interact (presenting both positive and negative feedbacks) with regional and global climate systems, so they must be evaluated within an integrated framework [6]. However, given the complexity and the lack of appropriate computer resources, traditional climate models strongly simplify the representation

of aerosol-radiation-cloud interactions. This has historically led to two independent disciplines: the climate modelling and the air quality communities, creating separate modelling systems that are only loosely coupled (the so-called offline models) [7].

It is nowadays widely known that realistic simulations of the combined aerosol-radiation (ARI) and aerosol-cloud interactions (ACI) require models where aerosols, meteorology/climatology, radiation, clouds, and chemistry are coupled in a fully interactive manner. Otherwise, offline models could lead to large inconsistencies. For instance, the constant droplet number assumed by offline models in order to close the equations describing cloud droplet radiation interactions forces the use of empirical relationships between aerosol number and the cloud droplet nucleation term [8]. The usage of such relations may induce inconsistencies between cloud mass and droplet number in a model [9]. Hence, fully coupled (online) climate/chemistry models must be used nowadays in order to reduce (or, at least, to characterize) the uncertainties in the representation of aerosol-cloud processes.

Thus, motivated by a better understanding of the impact of ARI and/or ACI on a regional scale, online chemistry/climate models with full couplings between the air quality and meteorological/climatological components have been developed and applied recently (e.g., [10–12]). A growing number of studies have recently started to address the coupling of aerosols and clouds in regional chemistry/climate models, coordinated through collaborative European projects from FP7 and Horizon 2020 (e.g., MACC), International programmes such as AQMEII [13–18]; or COST Actions like ES1004-EuMetChem [12,19,20]. However, as observed in the scientific literature, the application of regional chemistry/climate on-line coupled models is currently biased towards studies of isolated episodes (e.g., [21–24]) because of the demanding computational resources. Hence, previous works do not allow a representation of aerosol-cloud interactions for climate-representative time periods.

Therefore, the main objective of this work is to evaluate the added value provided by the inclusion of ACI with respect to a base case (where only ARI effects are taken into account) during a period covering the years 2003–2010. For that, a fully coupled (online) climate/chemistry model (WRF-Chem) allowing ARI and ACI effects has been used.

## 2. Materials and Methods

### *2.1. Model Configuration*

The regional climate simulations were carried out using the Weather Research Forecast (WRF) version 3.6.1 [25] and WRF model coupled with Chemistry (WRF-Chem) version 3.6.1 [26]. This model is widely used by the scientific community. For the historical period (2003–2010), the ERA20C reanalysis with a horizontal resolution of approximately 125 km [27] was used. The spatial Euro-CORDEX domain [28] covers Europe with a spatial resolution of 0.44° both in latitude and longitude. The meteorological boundary conditions were updated every 6 h [27], while aerosol/gas boundary conditions were taken from MOZART-4/GEOS-5 [29]. Outputs were recorded every hour. Twenty-nine inhomogeneous sigma levels were used vertically. The top level was defined at 50 hPa. The evolution of $CO_2$, $CH_4$, and $N_2O$ greenhouse gases were considered according to the recommendation of Jerez et al. [30]. The physics configuration consisted of: the Lin microphysics scheme [31], the Noah land surface model [32], the RRTM radiative scheme [33], the Grell 3D ensemble cumulus scheme [34,35] and the University of Yonsei boundary layer scheme [36].

Anthropogenic emissions coming from the Atmospheric Chemistry and Climate Model Intercomparison Project (ACCMIP) [37] were used, unchanged during the simulation period (e.g., [2,38,39]). Natural emissions depend on climate conditions and therefore vary with meteorological conditions (e.g., [5,40]).

The boundary conditions from the global model do not provide information on the Saharan dust. For this reason, we implemented two one-way nested domains. An outer 150 km spatial resolution covered the most important areas of Saharan dust emission [41–43]. As the task of this domain is to provide the boundary conditions, spectral nudging was used in the parent domain so that the

introduction of dust coincides with the synoptic situation. The nudging is applied between the top of the model and the planetary boundary layer to wind (vorticity and divergence), water vapour mixing ratio and temperature. The internal domain covers all of Europe and is established by Euro-CORDEX, as described before.

### *2.2. Aerosol Optical Depth (AOD) Simulations in WRF-Chem*

WRF-Chem model run with the GOCART aerosol module [44]. The simulated aerosols included five species, namely sulphate, mineral dust, sea salt aerosol, organic matter, and black carbon. Aerosol Optical Depth (AOD) has been externally prognosticated at 550 nm (AOD550) for different chemical species, including sulphate, mineral dust, sea salt aerosol, organic matter, and black carbon. AOD550 obtained from these species is denoted hereafter as AODSU, AODDU, AODSS, AODOM, and AODBC, respectively. Total AOD is abbreviated as AODTO. The GOCART scheme was coupled with RACM-KPP [45] as the gas-phase chemistry option; the Fast-J photolysis module was used as photolysis option [46]. Biogenic emissions were calculated using the Guenther scheme [47]. AOD550 was estimated using the reconstructed mass-extinction method [48,49], which has also been applied in other works covering Europe (e.g., [50,51]). The sum of the absorption ($\beta_a$) and the attenuation by scattering ($\beta_s$) gives the extinction coefficient ($\beta_{ext}$), which is a function of the wavelength ($\lambda$). The total AOD550 is the vertical integration (in our case, the addition) of the product of the extinction and the layer thickness ($\Delta Z_i$) for each $i$ layer, that is:

$$AOD550 = \sum_{i=1}^{N} (\beta_a + \beta_b)_i \Delta Z_i \quad (1)$$

where $\beta_{ext}$ ($m^{-1}$) is estimated using the following semiempirical approach depending on the aerosol mass and the relative humidity (RH):

$$\beta_a = 0.01[EC] \quad (2)$$

$$\beta_s = 0.003 f(RH)([NH_4^+] + [SO_4^{2-}] + [NO_3^-] + 0.004[OC] + 0.001[PM_{fine}] + 0.0006[PM_{coarse}] \quad (3)$$

where the concentrations are in mg $m^{-3}$ and all coefficients in the equation stand for the specific extinction cross section at 550 nm (in $m^2$ mg $m^{-1}$).

Two sets of climatic simulations were run: (1) including only aerosol-radiation interactions (ARI), which was considered to be the base case in our study; and (2) simulations including aerosol-cloud interactions (ARI+ACI, denoted afterwards as ACI for the sake of brevity). WRF-Chem aerosol-cloud-radiation interactions are explained in detail in Palacios-Peña et al. [12]. For ARI [46,52], each chemical constituent of the aerosol was associated with a complex index of refraction. The overall refractive index for a given size bin was determined by volume averaging. The Mie theory and the summation over all size bins were used to determine the composite aerosol optical properties. Wet particle diameters were used in the calculations. Finally, aerosol optical properties are transferred to the shortwave radiation scheme. ACI in WRF-Chem [52] were implemented by linking the simulated cloud droplet number with the microphysics schemes. Therefore, the droplet number affected both the calculated droplet mean radius and the cloud optical depth.

It should be noted that the WRF-Chem version used (3.6.1) does not allow a full coupling of aerosol-cloud interactions. For instance, the model distinguishes wet scavenging for large-scale and sub-grid stratiform and sub-grid convective clouds. Convective wet scavenging (conv_tr_wetscav) is not available in WRF-Chem when using GOCART. Moreover, in-cloud wet scavenging or cloud chemistry is also not available. So, the full description of ACI is not implemented in WRF-Chem. However, the microphysics implemented in the simulations rely on the Lin scheme [31,53], a single moment scheme that turns into a two moments scheme in the simulations denoted as ACI. Further detail on ACI implemented in the simulations are detailed below.

As aforementioned, the Lin scheme is a single moment scheme based on Lin et al. [31], including some modifications, such as saturation adjustment [54] and ice sedimentation, which is related to the sedimentation of small ice crystals [55]. It includes six classes of hydrometeors: water vapour, cloud water, rain, cloud ice, snow, and graupel. This scheme was one of the first to parameterize snow, graupel, and mixed-phase processes (such as the Bergeron process and hail growth by riming), and it has been widely used in numerical weather studies.

The one-moment microphysical scheme is unsuitable for assessing the aerosol-clouds interactions as it only predicts the mass of cloud droplets and does not represent the number concentration of cloud droplets [56]. The the prediction of two moments provides a more robust treatment of the particle size distributions, which is key for computing the microphysical process rates and cloud/precipitation evolution. Therefore, prediction of additional moments allows greater flexibility in representing size distributions and hence microphysical process rates.

In this sense, although the Lin microphysics is presented as a single moment scheme, the WRF-Chem model allows to transform the single into a double moment scheme. A prognostic treatment of cloud droplet number was added [57], which treats water vapour and cloud water, rain, cloud ice, snow, and graupel. The autoconversion of cloud droplets to rain droplets depends on droplet number [58]. Droplet-number nucleation and (complete) evaporation rates correspond to the aerosol activation and resuspension rates. Ice nuclei based on predicted particulates are not treated. However, ice clouds are included via the prescribed ice nuclei distribution following the Lin scheme. Finally, the interactions of clouds and incoming solar radiation have been implemented by linking simulated cloud droplet number with the Goddard shortwave radiation scheme, representing the first indirect effect, and with Lin microphysics, which represents the second indirect effect [25]. Therefore, droplet number will affect both the calculated droplet mean radius and cloud optical depth.

### *2.3. Copernicus Atmosphere Monitoring Service (CAMS) Reanalysis*

The estimations of AODSU, AODDU, AODSS, AODOM, AODBC, and AODTO (at 550 nm) were compared to the monthly information provided by Copernicus Atmosphere Monitoring Service (CAMS) reanalysis [59]. This reanalysis is the latest global reanalysis dataset of atmospheric composition produced by the European Centre for Medium-Range Weather Forecasts (ECMWF), consisting of three-dimensional time-consistent atmospheric composition fields, including aerosols and chemical species with a horizontal resolution of 80 km. This reanalysis has been extensively evaluated for aerosols and gas-phase pollutants against observations during the years 2003–2016 [59,60], finding an error generally ranging from 10% to 20%. Focusing on AOD, CAMS reanalysis improves the skill of other existing chemistry reanalyses when compared against AERONET observations, indicating a very slight negative monthly bias of $-0.007$ over Europe [59].

### *2.4. AErosol RObotic NETwork (AERONET)*

In addition to CAMS, daily data from the AErosol RObotic NETwork (AERONET) stations available during the target period (2003–2010) have been used to evaluate the AOD representation by CAMS and regional simulations (ARI-basecase and ACI). AOD at 675 nm (AOD675) is the evaluated variable because this wavelength is provided by a large number of stations (data is scarce at 550 nm). Model data (AOD550) has been estimated at 675 nm by using the Ångström exponent. Figure 1 shows AERONET stations represented by a number. The name, as well as the coordinates of the stations used, are listed in Table 1. AERONET observations come from Level 2.0 and their error is (under cloud-free conditions) $< \pm 0.01$ for $\lambda > 440$ nm and $< \pm 0.02$ for shorter wavelengths [61].

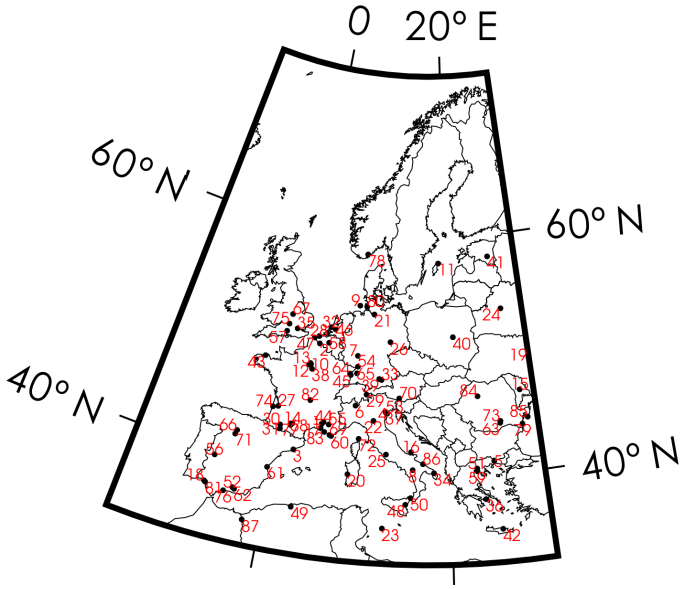


**Figure 1.** Location of AERONET stations used for the validation of modelling results. The number in the Figure corresponds to the stations detailed in Table 1, where stations are listed by code longitude, latitude, name, and corresponding number in this figure.

**Table 1.** Location, number, and name of all AERONET stations included in this contribution for AOD675 evaluation.

| Longitude | Latitude | N. | Name | Longitude | Latitude | N. | Name |
|---|---|---|---|---|---|---|---|
| 4.82 | 43.58 | 1 | La_Crau | 3.14 | 50.61 | 2 | Lille |
| 2.11 | 41.39 | 3 | Barcelona | 12.51 | 45.31 | 4 | Venise |
| 24.92 | 41.15 | 5 | Xanthi | 8.63 | 45.80 | 6 | Ispra |
| 8.30 | 50.00 | 7 | Mainz | 15.72 | 40.60 | 8 | IMAA_Potenza |
| 7.89 | 54.18 | 9 | Helgoland | 2.44 | 48.79 | 10 | Creteil |
| 18.95 | 57.92 | 11 | Gotland | 2.21 | 48.71 | 12 | Palaiseau |
| 2.36 | 48.85 | 13 | Paris | 1.48 | 43.56 | 14 | Toulouse |
| 28.82 | 47.00 | 15 | Moldova | 15.49 | 42.12 | 16 | Tremiti |
| 4.88 | 43.93 | 17 | Avignon | −6.73 | 37.10 | 18 | El_Arenosillo |
| 30.50 | 50.36 | 19 | Kyiv | 8.50 | 39.91 | 20 | IMC_Oristano |
| 9.97 | 53.57 | 21 | Hamburg | 10.95 | 44.63 | 22 | Modena |
| 12.63 | 35.52 | 23 | Lampedusa | 27.60 | 53.92 | 24 | Minsk |
| 12.65 | 41.84 | 25 | Rome_Tor_Vergata | 12.44 | 51.35 | 26 | Leipzig |
| −0.58 | 44.79 | 27 | Bordeaux | 2.92 | 51.23 | 28 | Oostende |
| 9.84 | 46.81 | 29 | Davos | 0.08 | 43.25 | 30 | Tarbes |
| 0.14 | 42.94 | 31 | Pic_du_Midi | 4.33 | 52.11 | 32 | The_Hague |
| 11.57 | 48.15 | 33 | Munich_University | 18.11 | 40.34 | 34 | Lecce_University |
| −0.13 | 51.52 | 35 | London-UCL-UAO | 23.72 | 37.97 | 36 | Athens-NOA |
| 12.33 | 45.44 | 37 | ISDGM_CNR | 2.68 | 48.41 | 38 | Fontainebleau |
| 11.26 | 48.21 | 39 | Munich_Maisach | 20.79 | 51.84 | 40 | Belsk |
| 26.47 | 58.26 | 41 | Toravere | 25.28 | 35.33 | 42 | Forth_Crete |
| −3.46 | 48.73 | 43 | Lannion | 5.06 | 44.08 | 44 | Carpentras |
| 7.62 | 48.34 | 45 | Rossfeld | 4.93 | 51.97 | 46 | Cabauw |
| 2.37 | 51.04 | 47 | Dunkerque | 15.02 | 37.61 | 48 | Etna |
| 2.88 | 36.51 | 49 | Blida | 15.57 | 38.20 | 50 | Messina |
| 22.96 | 40.63 | 51 | Thessaloniki | −3.60 | 37.16 | 52 | Granada |
| 12.38 | 45.43 | 53 | Nicelli_Airport | 8.43 | 49.09 | 53 | Karlsruhe * |
| 5.71 | 43.94 | 55 | OHP_Observatoire | −6.34 | 39.48 | 56 | Caceres |
| −1.44 | 51.14 | 57 | Chilbolton | 4.35 | 50.78 | 58 | Brussels |
| 22.98 | 40.38 | 59 | Epanomi | 6.16 | 43.00 | 60 | Porquerolles |
| −0.42 | 39.51 | 61 | Burjassot | −3.39 | 37.06 | 62 | Dilar |
| 26.03 | 44.35 | 63 | Bucharest_Inoe | 7.54 | 48.44 | 64 | Obernai |

**Table 1.** *Cont.*

| Longitude | Latitude | N. | Name | Longitude | Latitude | N. | Name |
|---|---|---|---|---|---|---|---|
| 8.40 | 48.54 | 65 | Black_Forest_AMF | −4.60 | 42.00 | 66 | Autilla |
| −1.12 | 52.62 | 67 | Leicester | 1.28 | 43.38 | 68 | Le_Fauga |
| 5.94 | 43.07 | 69 | Saint_Mandrier | 13.90 | 46.68 | 70 | Kanzelhohe_Obs |
| −4.71 | 41.66 | 71 | Valladolid_Sci | 9.36 | 43.00 | 72 | Ersa |
| 26.08 | 44.51 | 73 | Baneasa | −1.16 | 44.66 | 74 | Arcachon |
| −1.33 | 51.77 | 75 | Wytham_Woods | −4.48 | 36.72 | 76 | Malaga |
| 1.26 | 43.50 | 77 | Seysses | 8.25 | 58.39 | 78 | Birkenes |
| 28.63 | 44.08 | 79 | Eforie | 8.88 | 54.13 | 80 | Buesum |
| −6.57 | 37.02 | 81 | Huelva | 3.11 | 45.76 | 82 | Aubiere_LAMP |
| 5.29 | 43.27 | 83 | Frioul | 23.55 | 46.77 | 84 | Cluj_UBB |
| 29.36 | 44.60 | 85 | Gloria | 16.88 | 41.11 | 86 | Bari_University |
| −1.90 | 34.65 | 87 | Oujda | | | | |

* Two stations available.

### *2.5. Previous Validation Results*

The results of the modelling system presented here have been extensively evaluated in previous works. In this sense, the simulations have been compared to the remote-sensing data from the Moderate Resolution Imaging Spectroradiometer (MODIS) sensors aboard the Terra and Aqua platforms (MOD04_L2 and MYD04_L2) from collection six (C6) [18], finding that large underestimations in the simulations can be related to the misrepresentation of black carbon coming from biomass burning episodes. Also, the slight underestimations found for AODTO can be ascribed to a misrepresentation of the aerosol vertical profile modelled in these simulations [12].

The evaluation of meteorological fields indicate that maximum and mean temperatures were underestimated in the simulations [19] when compared to the E-OBS database [62]. In addition, these authors found no straightforward conclusion with respect to the improvement (or not) of the bias when introducing ACI interactions with respect to ARI results (bias of −0.696 K in mean temperature in ARI simulations and −0.642). However, very important improvements were found for the spatiotemporal representation of the temperature when ACI simulations were compared to ARI.

Regarding cloud properties, Baró et al. [20] found that an underestimation(overestimation) of cloud fraction (CF) is observed over land(sea) areas. The model simulations present a positive bias close to 40% over the sea, while a negative bias over −35% is over the land. While the negative bias may be due to the general underestimation in the cloud condensation nuclei representation by the models (that can be slightly corrected when introducing ACI in the simulations) [63], the overestimations found offshore might be related to satellite retrievals missing thin clouds [20,64]. Also, these authors found an underestimation of the cloud liquid water path (CLWP) related to the lower number of cloud droplets provided by the Lin microphysics schemes when compared to other microphysics schemes (e.g., [15,65]).

## 3. Results

### *3.1. AOD AERONET Evaluation*

Figure 2a displays average monthly AERONET AOD675 during the target period. Temporal and spatial mean of observed AOD675 is 0.12. Stations with lower AOD675 values (below 0.05) are located in rural areas as Autilla (66, Iberian Peninsula); Pic de Midi (31, Pyrenees); Aubiere (82, France); or Davos (29, Switzerland). This is an expected fact since these are background stations, located principally in rural areas where lower aerosol loads from anthropogenic origin are expected. A particular station is Bordeaux (27, France) with mean AOD675 values of 0.04 as a consequence of the high precipitation frequency fluxes over this area [66]. On the other hand, the highest AOD values (above 0.20) were found in Tarbes (30, France); Gloria (85, Romania); and Rossfeld (45, Germany) because these areas present an important anthropogenic pollution, especially associated to black carbon [39,67].

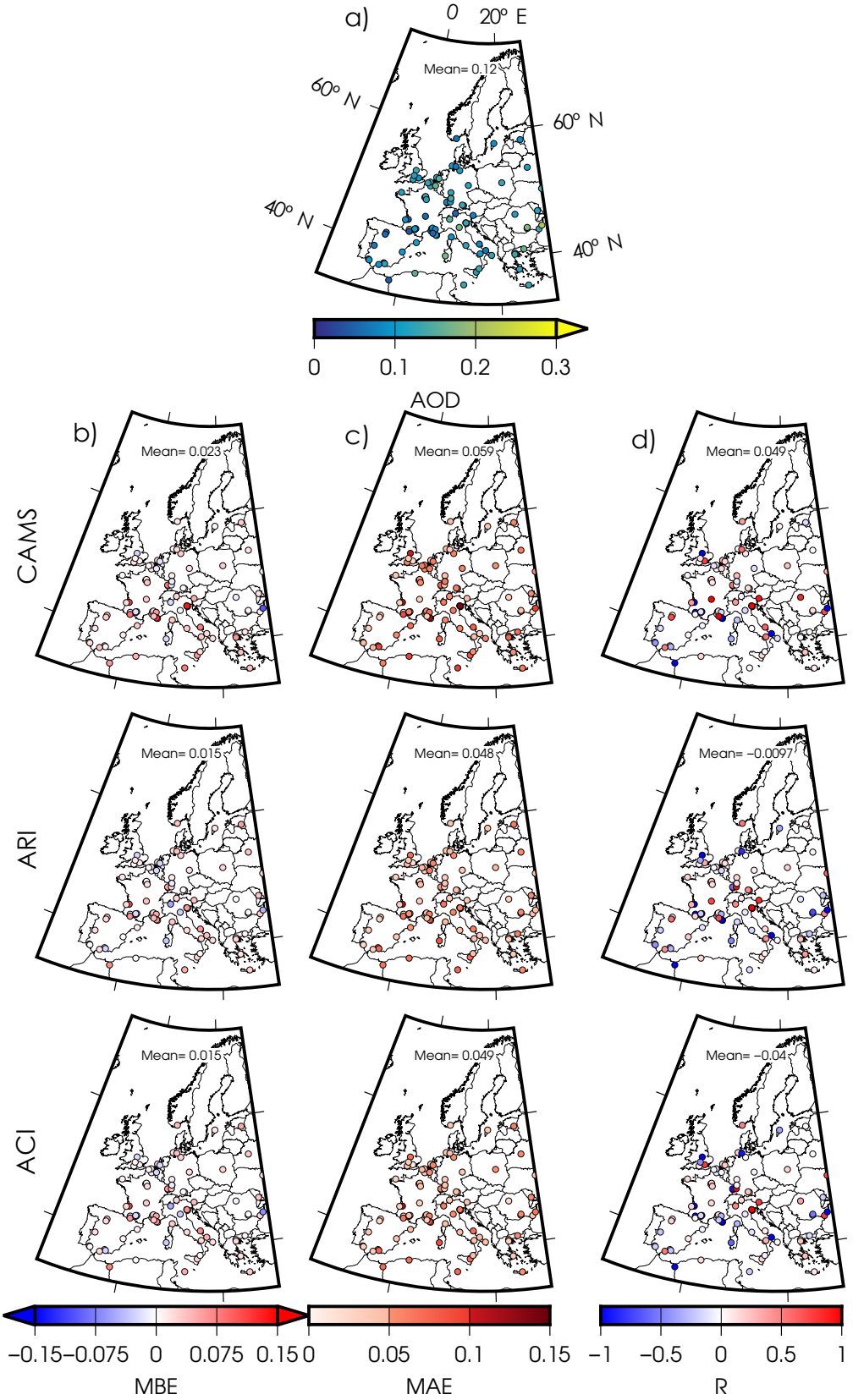


**Figure 2.** (**a**) Mean monthly aerosol optical depth (AOD) at 670 nm from AERONET, averaged for the target period. (**b**) Mean bias error (MBE); (**c**) mean absolute error (MAE), and (**d**) temporal correlation for Copernicus Atmosphere Monitoring Service (CAMS) (R) (top), ARI-base case (centre) and aerosol-cloud interactions (ACI) simulation (bottom).

Medium AOD values are found in the many European cities as Belsk (40, Poland); Kyiv (19, Ukraine); Mainz, Leipzig, and Karlrsuhe (7, 26, 52, Germany), Paris metropolitan area (10, 12, 13, France); southwest of Great Britain and Benelux cities and all the cities bordering the Mediterranean. These levels could also be attributed to high aerosol loads from anthropogenic origin, since these areas are far from natural influences. However, in more southern locations like the Mediterranean, AOD675 levels could also come from recurrent desert dust outbreaks [68,69].

When mean bias error (MBE) and mean average error (MAE) are analyzed (Figure 2b,c) there is a general slight overestimation. Only 13% of the stations used underestimate AOD675 for the CAMS reanalysis. The skill of the model improves in regional simulations (ARI and ACI) with respect to CAMS reanalysis for both statistical figures. Temporal and spatial MBE mean is 0.023 for CAMS, while the bias error reduces to 0.015 for both regional simulations. On the other hand, MAE mean is 0.059 for CAMS, 0.048 for ARI (base case) and 0.049 for ACI. According to these results, the ARI and ACI simulation present a significant improvement in the absolute error with respect to the global CAMS reanalysis, while no significant differences are found between ARI and ACI.

The aforementioned analysis is representative of the average behavior of most of the stations, but some of them should be highlighted. In Bordeaux (27, France), MBE(MAE) reaches values of 0.113(0.113), 0.107(0.107), and 0.112(0.112) for CAMS, ARI, and ACI, respectively, showing a better representation of AOD by ARI simulations and no significant improvement for ACI. Another station to highlight is Oujda (87, Morocco) with MBE(MAE) of −0.099(0.99) for CAMS, while the error reduces to 50% in ARI, −0.045(0.045); and 33% for ACI: −0.066(0.066). The rest of the stations display MBE and MAE under 0.1, with similar values for both statistics. The fact that bias and error are identical in absolute value means that the bias is always produced in the same direction (always under- or overestimation) for each station. A small number of stations exhibit an MBE for regional coupled simulations higher than CAMS (3% and 31% of the stations), but these differences are usually negligible (±0.01).

With respect to the time correlation coefficient ($r$), the time series have been normalized before estimating the correlation (that is, the annual cycle has been removed, so that the correlation is not influenced by the seasonality of the signal). Results indicate that there is not a clear behaviour that can lead to the definition of some added value of regional simulations over CAMS or ARI vs. ACI (Figure 2d). More than 50% of AERONET stations display low correlation values with modelled data. However, correlations are higher for regional climate simulations with WRF-Chem (ARI and ACI). Around 10% of stations show values higher than 0.5 when CAMS is evaluated while 15% of the stations do for ARI and 13% for ACI.

### *3.2. Biases and Improvement of the Absolute Errors in the Simulations Including Aerosol-Cloud Interactions*

Figure 3 depicts the bias error of the different modelled AOD550 climatologies when assessed against the CAMS reanalysis, the bias of the ARI-base case simulations and the improvement of the error with respect to the base case simulation when including ACI. The improvement of the error is defined as:

$$IE = |ARI_s - CAMS_s| - |ACI_s - CAMS_s| \quad (4)$$

where $s$ denotes the AOD at 550 nm for each chemical species $s$ (total AOD, sulphate, dust, sea salt, organic matter, or black carbon). The AOD provided by CAMS reanalysis is taken in this section as the benchmark to compare our simulations. Henceforth, Equation (4) reflects that a positive number is indicative of a higher error in the ARI-base case simulation; that is, the error against CAMS is reduced when introducing ACI in our simulations. Conversely, negative values of IE indicate worse skills when aerosol-cloud interactions are included in regional simulations.

The evaluation results compare the climatologies taken from CAMS reanalysis (Figure 3a) with the base case simulation. In general, the bias error of the simulations (Figure 3b) show an excellent agreement between all the species and CAMS-derived AOD variables, but with a general underestimation of AODTO (−7.62%) over the entire domain. This result is in agreement with those of

previous works [20,70]. The bias for AODTO is higher in northern Africa, caused by the pervasive underestimation of the aerosol load coming from the Sahara desert (AODDU is underestimated by 0.02–0.04 in this area, representing an underestimation of over 20% of AOD). However, AODDU in northern Europe is slightly overestimated, especially over the northeastern part of the domain, caused by the unrealistic high values of dust coming from the Gobbi desert through the boundary conditions [12,18].

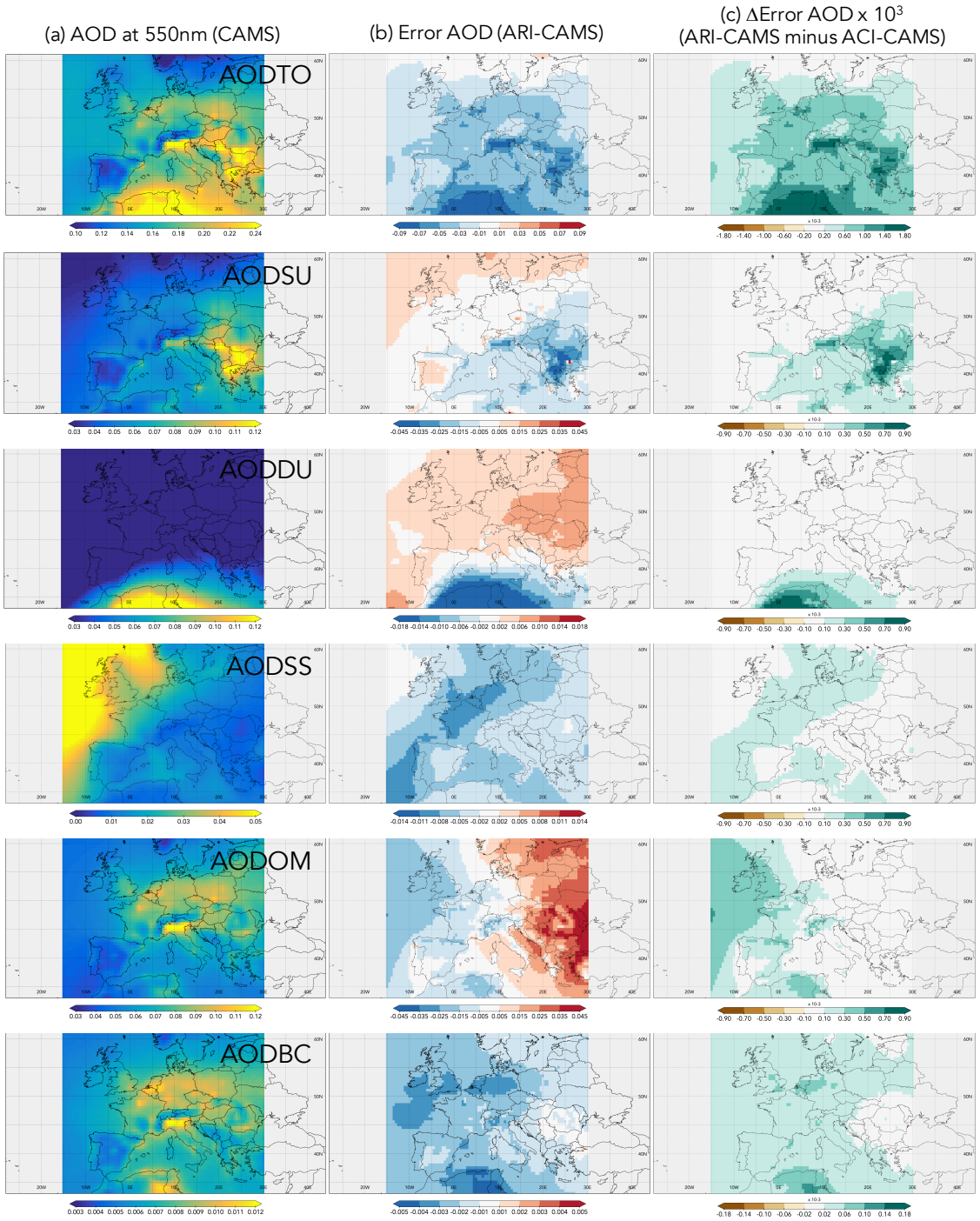


**Figure 3.** (From top to bottom: AODTO, AODSU, AODDU, AODSS, AODOM, AODBC). (**a**) CAMS reanalysis climatology of AOD at 550 nm. (**b**) Error (bias) of the simulation for the base case and (ARI). (**c**) Improvement of the error with respect to the base case simulation when including ACI. A positive number, represented by green colours, indicates a reduction of the absolute error in ACI simulations with respect to the base case.

AODSU presents a slight underestimation (Table 2) both in ARI ($-0.64 \times 10^{-3}$) and ACI simulations ($-0.55 \times 10^{-3}$), especially over eastern Europe, which can be related to a strong underestimation of winter sulphate aerosol [71,72]. Similarly, AODSS and AODBC depict a tendency towards underestimation in ARI-base case simulation ($-4.79$ and $-1.89 \times 10^{-3}$, respectively), while AODOM is overestimated in ARI simulation ($3.21 \times 10^{-3}$ averaged over the domain).

With respect to the improvement of the error (IE), our results in Figure 3 and Table 2 indicate a positive value, meaning that a reduction in the error is found for ACI simulations for all chemical species. ACI have a strong effect on particulate matter and AOD coming from different species, also conditioning the emissions of natural aerosols (sea salt, mineral dust, which strongly depend on wind speed) [73,74], atmospheric transport, and chemistry of large emitting sources, such as plumes from forest fires and cities [75]. It is noticeable, the improvement of AODDU, the error of which improves by $0.05 \times 10^{-3}$, that is, an improvement of 20.22% in the error of ARI-base case simulations. This improvement, as discussed later, is especially caused by the reduction of the error over northern Africa. Also, AODSU reduces the error by 14.06%, as a consequence of an enhanced oxidation of sulphate (higher concentrations of hydroxyl radical) when including ACI. For the rest of the chemical components, inclusion of ACI reduces the error by lower than 5% (2.09% for AODSS, 3.42% for AODOM, and 2.11% for AODBC).

**Table 2.** Mean values of Aerosol Optical Depth at 550 nm (unitless) for the CAMS reanalysis in the domain; bias of the simulation for the base case (ARI) and improvement of the error with respect to the base case simulation when including ACI. A positive value of the improvement indicates a reduction of the error in the ACI simulation with respect to the base case.

| | **AOD CAMS rean.** $\times$ **10**$^{-3}$ | **Bias ARI** $\times$ **10**$^{-3}$ | **IE** $\times$ **10**$^{-3}$ **(unitless and %)** |
|---|---|---|---|
| Total AOD at 550 nm | 207.21 | −7.61 | 0.58 (7.62%) |
| Sulphate AOD at 550 nm | 49.81 | −0.64 | 0.09 (14.06%) |
| Dust AOD at 550 nm | 23.29 | 0.25 | 0.05 (20.22%) |
| Sea Salt AOD at 550 nm | 25.29 | −4.79 | 0.10 (2.09%) |
| Organic Matter AOD at 550 nm | 58.23 | 3.21 | 0.11 (3.42%) |
| Black Carbon AOD at 550 nm | 6.59 | −1.89 | 0.04 (2.11%) |

### *3.3. Correlation Coefficients and Their Improvements When Including Aerosol-Cloud Interactions*

Figure 4a shows the time correlation coefficients ($r$) between the base case simulation (ARI) and CAMS reanalysis. It should be pointed out that, as done in Section 3.1, the annual cycle of the series have been removed before estimating the $r$. In general, the best correlation coefficients are estimated for the southern and south-eastern part of the target domain, with $r > 0.80$ for all chemical species, while the poorest correlations are calculated over the Scandinavian peninsula and the northeastern part of the domain, where $r < 0.1$ for several species as AODOM and AODDU. The $r$ coefficients, averaged for the entire domain (Table 3) range from 0.495 in the case of AODOM to 0.771 for AODSS, depending on the individual component. The AODTO vary from 0.124 in the northeastern part of the domain (near the boundaries) to 0.942 in the Mediterranean sea, where the correlation coefficients for AODTO are strongly related to the ability of the WRF-Chem simulations to reproduce the spatio-temporal variability of sea salt aerosol.

Moreover, the lowest correlation coefficient in the case of AODOM is caused by the limited skill of the model to reproduce the optical depth associated to organic aerosols in the northeastern part of the domain ($r < 0.1$); this is also where the model presents the highest bias errors for this species. Overseas, the AODOM ranges between 0.50 and 0.70, pointing out to a good representation of the time variation of AODOM over the Mediterranean and the Atlantic Ocean.

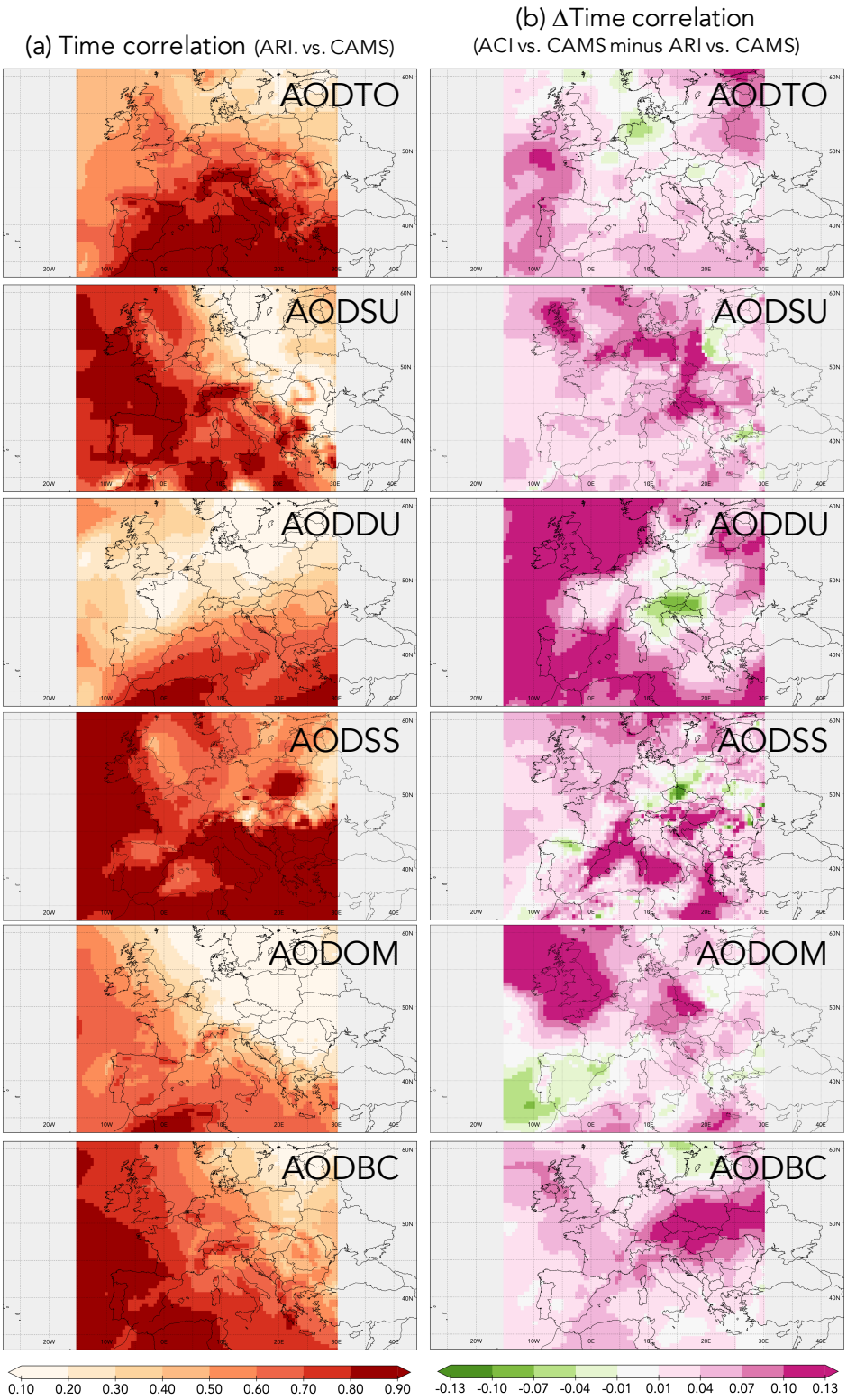


**Figure 4.** (From top to bottom: AODTO, AODSU, AODDU, AODSS, AODOM, AODBC). (**a**) Pearson correlation coefficient of base case simulations (ARI) with CAMS reanalysis for AOD at 550 nm. (**b**) Improvement in the correlation coefficient when including aerosol-cloud interactions with respect to the base case simulation. A positive(negative) number, represented by pink(green) colours, indicates a higher(lower) correlation coefficient in ACI simulations with respect to the base case.

Regarding the improvement of the correlation coefficient when including ACI in the simulations (Figure 4b), the behaviour is similar to the case for the IE. The total correlation coefficient improves by 8%, averaged for all the domain, with slight decreases in the values of *r* over the Netherlands and nortwestern Germany. The largest improvement in the simulation is found for AODDU, where *r* increases by nearly 20% when including aerosol-cloud interactions (Table 3), mainly because of the improvements of the correlation coefficients over western and southern Europe (slight decreases of the *r* are found over the central part of the simulation domain). There is a better correlation in the rest of the chemical components when ACI are introduced in the models, ranging from an improvement of 6% for AODBC and AODSU to 9% for AODSS and AODOM. The better correlation coefficients found do not present a homogeneous behaviour over the entire domain. For instance, for AODOM strongly increases over the British Isles, while decreases over the Iberian Peninsula. For AODBC, it is strongly noticeable that the largest improvements are found over those areas with the largest emitting sources (central and eastern Europe), with increases of 0.10 over those areas where the correlation coefficient is lower (0.20–0.30), thus showing improvements of 50% in the correlation coefficient.

**Table 3.** Mean values of Pearson time correlation coefficients for Aerosol Optical Depth at 550 nm (AOD550) for the base case simulation (ARI) with the CAMS reanalysis and improvement of the Pearson correlation coefficient with respect to the base case simulation when including ACI. A positive value of the improvement indicates an increase in the correlation in the ACI simulation with respect to the base case.

| | **Correlation ARI** | **Improv. (unitless and %)** |
|---|---|---|
| Total AOD at 550 nm | 0.701 | 0.055 (7.86%) |
| Sulphate AOD at 550 nm | 0.725 | 0.048 (6.62%) |
| Dust AOD at 550 nm | 0.506 | 0.100 (19.77%) |
| Sea Salt AOD at 550 nm | 0.771 | 0.068 (8.82%) |
| Organic Matter AOD at 550 nm | 0.495 | 0.044 (8.89%) |
| Black Carbon AOD at 550 nm | 0.736 | 0.042 (5.71%) |

## 4. Discussion

The base case simulations (ARI) for the period 2003–2010 underestimate AODTO by 4% when compared with CAMS reanalysis (AODTO of 0.207 in CAMS, bias error of 0.008), which is in the same range as the bias found in other works. For instance, Baró et al. [20] found that, over Europe, moderately to largely underestimations are expected for aerosols loadings and AOD for most simulations from regional chemistry transport models. In this same sense, Lapina et al. [76] found out that GEOS-Chem underestimates the mean AOD value for the marine environment by 21%. Other works (such as Balzarini et al. [77]) indicate that, albeit different models trust different chemical mechanisms for reproducing aerosol optical properties, the AODTO is generally underestimated. These discrepancies could be studied in further works through sensitivity analysis, but the general trend for underestimations of AODTO in WRF-Chem simulations can be assigned to underpredictions in the aerosol dry mass by the models, an underestimation of the fraction of particles for a given mass, or to a misleading representation of the water associated with aerosols [69].

Focusing on the comparison with remote sensing observations, Pozzer et al. [70] compared AOD climate simulations to AERONET observations, finding that biases vary between 0.02 and 0.03. Hence, regional online coupled models improve those values, with AOD biases of 0.015 for both ARI and ACI simulations, a bias 50% lower than that found for global models as a consequence of the higher resolution used in regional models. In addition, Palacios et al. [18] used an ensemble of models from AQMEII Phase 3 [17] to assess AODTO against in-situ and remote sensing observations, finding out that the biases of the ensemble of AQMEII simulations when representing AOD are in the order of 0.05. In this sense, the bias observed in our evaluation is again lower than those found in the literature, pointing out to an accurate skill of the model when reproducing aerosol climatologies

over the European area. However, this improvement is not that evident for the correlation coefficient, which does not show a clear spatial pattern. This fact could be ascribed to the use of a monthly temporal resolution for the estimation of *r*, reducing the number of occurrences and hence hampering the estimation of an accurate correlation.

Apart from AODTO, scientific literature is much more limited when assessing chemical components of the AOD. In the case of AODSU, the underestimation found in ARI-base case could be related to two causes: (1) the pervasive tendency of regional models to be geographically biased by strong winter underestimations of sulphate concentrations at eastern European locations (it is widely known that the winter underestimation of sulphate is a common issue in most models that operate over Europe, which represent a direct couplet of sulfur chemistry with photochemistry) [71]; and (2) the fact that sulphate formation in the modelling systems is often limited by oxidant availability [72]. With respect to the AODOM, the inclusion of a complex organic aerosols mechanism in models (such as the mechanism used here) leads to a better agreement over certain areas over the sea (for instance, over the Atlantic ocean, as observed here in our simulations) but leads to overestimates of OM in other regions [76].

With respect to the improvement of the simulations when including ACI, there is a general improvement in the error of AODTO and correlation coefficients (around 8% for AODTO, over 20% in the case of AODDU) when compared with CAMS. Since the model generally underpredicts the CAMS concentrations, the inclusion of aerosol-cloud interactions can have an important effect increasing relative humidity [24], modifying the size of the particles due to hygroscopic growth, and hence, the AOD predictions, especially for hydrophilic species.

The improvement of the errors found here for the improvement of the AOD during the 2003–2010 period agrees with the results of other works for episodic studies (e.g., [18,19,23]). These works indicate that minor, but statistically significant, improvements are observed in AODTO and other climatic variables such as 2-m temperature when ACI processes and feedbacks are taken into account. For instance, improvements in AODTO around 12% during an episode of the Saharan dust outbreak over Europe in October 2010 when including ACI in an ensemble of models run under the EuMetChem initiative [12,19]. Moreover, these latter authors found an improvement of the error of 11% when ACI were included in WRF-Chem during the Russian 2010 heatwave episode (July 2010), even over areas far from wildfires emissions [12].

Hence, the IE is especially noticeable in the case of natural aerosols (dust and sea salt, of which emissions strongly depend on wind speed), as indicated in previous scientific literature [78,79]. As seen in Figure 3, there is a strong underestimation of AODDU over the southern part of the domain. ACI simulations provide a slight increase of wind speed over the Atlantic and southern part of the domain. This is a striking feature, found not only in our simulations but in other WRF-Chem simulations, including ACI (e.g., [19,24]), as a consequence of the strong increase in solar radiation over those target areas. Simulated cloud droplet numbers are between 5 and 100 $cm^3$ when ACI are taken into account over remote areas as the Atlantic ocean. If simulated aerosol concentrations are not taken into account for cloud droplet formation (as this is the case of our ARI-base case simulations), a standard value of 250 cloud droplets per $cm^3$ is assumed for the entire modelling domain, coming from the standard configuration of WRF and WRF-Chem [16]. Hence, the reduced number of cloud droplets over the Atlantic reduced cloudiness, increases solar radiation and the higher solar radiation enhances temperature and therefore winds, which promote the emission of dust and sea salt and therefore increase the AODDU and AODSS in our ACI simulations, reducing the negative bias found for dust over northern Africa and for sea salt over the entire domain.

Finally, it should be highlighted that the results found here may point to some benefits of including ACI when representing aerosol climatologies over Europe. The improvement of the skills in the simulations (around 8% for AODTO, reaching 20% for dust bias) could make climate scientists consider the inclusion of ACI in climate simulations, despite the larger computation required (higher by

a factor of eight with respect to the base case simulations) and considering the feedbacks of air pollution in the calculation of meteorological fields in coupled chemistry/climate regional models.

**Author Contributions:** Conceptualization, P.J.-G., J.P.M. and L.P.-P.; methodology, L.P.-P., J.P.M., J.M.L.-R., S.J., J.J.G.-N., R.L.-P., J.R. and P.J.-G.; software, J.M.L.-R. and S.J.; validation, P.J.-G. and L.P.-P.; formal analysis, L.P.-P., J.P.M., J.M.L.-R., S.J., J.J.G.-N., R.L.-P., J.R. and P.J.-G.; investigation, L.P.-P., J.P.M., J.M.L.-R., S.J., J.J.G.-N., R.L.-P., J.R. and P.J.-G.; writing–original draft preparation, L.P.-P. and P.J.-G.; writing–review and editing, L.P.-P., J.P.M., J.M.L.-R., S.J., J.J.G.-N., R.L.-P., J.R. and P.J.-G..; visualization, L.P.-P., J.J.G.-N.; supervision, P.J.-G.; project administration, P.J.-G.; funding acquisition, P.J.-G., J.P.M. All authors have read and agreed to the published version of the manuscript.

**Funding:** This research was funded by the European Regional Development Fund-Fondo Europeo de Desarrollo Regional (ERDF-FEDER), Spanish Ministry of Economy and Competitivity grant number CGL2017-87921-R (ACEX project), Spanish Ministry of Science, Innovation and Universities grant number RTI2018-100870-A-I00 (EASE project) and CLIMAX project (20642/JLI/18) funded by the Seneca Foundation-Agency for Science and Technology in the Region of Murcia.

**Conflicts of Interest:** The authors declare no conflict of interest.

## Abbreviations

The following abbreviations are used in this manuscript:

| | |
|---|---|
| ACI | Aerosol-cloud interactions |
| AOD | Aerosol optical depth |
| AOD550 | Aerosol optical depth at 550 nm |
| AOD675 | Aerosol optical depth at 675 nm |
| AODTO | Total aerosol optical depth at 550 nm |
| AODSU | Sulphate aerosol optical depth at 550 nm |
| AODDU | Dust aerosol optical depth at 550 nm |
| AODSS | Sea salt aerosol optical depth at 550 nm |
| AODOM | Organic aerosol optical depth at 550 nm |
| AODBC | Black carbon optical depth at 550 nm |
| AQCI | Air quality-climate interactions |
| ARI | Aerosol-radiation interactions |
| CAMS | Copernicus Atmosphere Monitoring Service |
| IE | Improvement of the error |
| MAE | Mean average error |
| MBE | Mean bias error |
| *r* | Correlation coefficient |

## References

1. Jacob, D.J.; Winner, D.A. Effect of climate change on air quality. *Atmos. Environ.* **2009**, *43*, 51–63. [CrossRef]
2. Jiménez-Guerrero, P.; Montávez, J.P.; Gómez-Navarro, J.J.; Jerez, S.; Lorente-Plazas, R. Impacts of climate change on ground level gas-phase pollutants and aerosols in the Iberian Peninsula for the late XXI century. *Atmos. Environ.* **2012**, *55*, 483–495. [CrossRef]
3. Juda-Rezler, K.; Reizer, M.; Huszar, P.; Krüger, B.C.; Zanis, P.; Syrakov, D.; Katragkou, E.; Trapp, W.; Melas, D.; Chervenkov, H.; et al. Modelling the effects of climate change on air quality over Central and Eastern Europe: Concept, evaluation and projections. *Clim. Res.* **2012**, *53*, 179–203. [CrossRef]
4. Kinney, P.L. Interactions of Climate Change, Air Pollution, and Human Health. *Curr. Environ. Health Rep.* **2018**, *5*, 179–186. [CrossRef] [PubMed]
5. Jiménez-Guerrero, P.; Gómez-Navarro, J.J.; Baró, R.; Lorente, R.; Ratola, N.; Montávez, J.P. Is there a common pattern of future gas-phase air pollution in Europe under diverse climate change scenarios? *Clim. Chang.* **2013**, *121*, 661–671. [CrossRef]
6. Alapaty, K.; Mathur, R.; Pleim, J.; Hogrefe, C.; Rao, S.T.; Ramaswamy, V.; Galmarini, S.; Schaap, M.; Makar, P.; Vautard, R.; et al. New Directions: Understanding interactions of air quality and climate change at regional scales. *Atmos. Environ.* **2012**, *49*, 419–421. [CrossRef]

7. Grell, G.; Baklanov, A. Integrated modeling for forecasting weather and air quality: A call for fully coupled approaches. *Atmos. Environ.* **2011**, *45*, 6845–6851. [CrossRef]
8. Storelvmo, T.; Kristjansson, J.E.; Lohmann, U. Aerosol Influence on Mixed-Phase Clouds in CAM-Oslo. *J. Atmos. Sci.* **2008**, *65*, 3214–3230. [CrossRef]
9. Baklanov, A.; Schlünzen, K.; Suppan, P.; Baldasano, J.; Brunner, D.; Aksoyoglu, S.; Carmichael, G.; Douros, J.; Flemming, J.; Forkel, R.; et al. Online coupled regional meteorology chemistry models in Europe: Current status and prospects. *Atmos. Chem. Phys.* **2014**, *14*, 317–398. [CrossRef]
10. Nabat, P.; Somot, S.; Mallet, M.; Sevault, F.; Chiacchio, M.; Wild, M. Direct and semi-direct aerosol radiative effect on the Mediterranean climate variability using a coupled regional climate system model. *Clim. Dyn.* **2015**, *44*, 1127–1155. [CrossRef]
11. Revell, L.E.; Stenke, A.; Luo, B.; Kremser, S.; Rozanov, E.; Sukhodolov, T.; Peter, T. Impacts of Mt Pinatubo volcanic aerosol on the tropical stratosphere in chemistry–climate model simulations using CCMI and CMIP6 stratospheric aerosol data. *Atmos. Chem. Phys.* **2017**, *17*, 13139–13150. [CrossRef]
12. Palacios-Peña, L.; Baró, R.; Baklanov, A.; Balzarini, A.; Brunner, D.; Forkel, R.; Hirtl, M.; Honzak, L.; López-Romero, J.M.; Montávez, J.P.; et al. An assessment of aerosol optical properties from remote-sensing observations and regional chemistry–climate coupled models over Europe. *Atmos. Chem. Phys.* **2018**, *18*, 5021–5043. [CrossRef]
13. Rao, S.T.; Galmarini, S.; Puckett, K. Air Quality Model Evaluation International Initiative (AQMEII): Advancing the State of the Science in Regional Photochemical Modeling and Its Applications. *Bull. Am. Meteorol. Soc.* **2011**, *92*, 23–30. [CrossRef]
14. Solazzo, E.; Bianconi, R.; Pirovano, G.; Matthias, V.; Vautard, R.; Moran, M.D.; Appel, K.W.; Bessagnet, B.; Brandt, J.; Christensen, J.H.; et al. Operational model evaluation for particulate matter in Europe and North America in the context of AQMEII. *Atmos. Environ.* **2012**, *53*, 75–92. [CrossRef]
15. Baró, R.; Jiménez-Guerrero, P.; Balzarini, A.; Curci, G.; Forkel, R.; Grell, G.; Hirtl, M.; Honzak, L.; Langer, M.; Pérez, J.L.; et al. Sensitivity analysis of the microphysics scheme in WRF-Chem contributions to AQMEII phase 2. *Atmos. Environ.* **2015**, *115*, 620–629. [CrossRef]
16. Forkel, R.; Balzarini, A.; Baró, R.; Bianconi, R.; Curci, G.; Jiménez-Guerrero, P.; Hirtl, M.; Honzak, L.; Lorenz, C.; Im, U.; et al. Analysis of the WRF-Chem contributions to AQMEII phase2 with respect to aerosol radiative feedbacks on meteorology and pollutant distributions. *Atmos. Environ.* **2015**, *115*, 630–645. [CrossRef]
17. Galmarini, S.; Koffi, B.; Solazzo, E.; Keating, T.; Hogrefe, C.; Schulz, M.; Benedictow, A.; Griesfeller, J.J.; Janssens-Maenhout, G.; Carmichael, G.; et al. Technical note: Coordination and harmonization of the multi-scale, multi-model activities HTAP2, AQMEII3, and MICS-Asia3: Simulations, emission inventories, boundary conditions, and model output formats. *Atmos. Chem. Phys.* **2017**, *17*, 1543–1555. [CrossRef]
18. Palacios-Peña, L.; Jiménez-Guerrero, P.; Baró, R.; Balzarini, A.; Bianconi, R.; Curci, G.; Landi, T.C.; Pirovano, G.; Prank, M.; Riccio, A.; et al. Aerosol optical properties over Europe: An evaluation of the AQMEII Phase 3 simulations against satellite observations. *Atmos. Chem. Phys.* **2019**, *19*, 2965–2990. [CrossRef]
19. Baró, R.; Palacios-Peña, L.; Baklanov, A.; Balzarini, A.; Brunner, D.; Forkel, R.; Hirtl, M.; Honzak, L.; Pérez, J.L.; Pirovano, G.; et al. Regional effects of atmospheric aerosols on temperature: An evaluation of an ensemble of online coupled models. *Atmos. Chem. Phys.* **2017**, *17*, 9677–9696. [CrossRef]
20. Baró, R.; Jiménez-Guerrero, P.; Stengel, M.; Brunner, D.; Curci, G.; Forkel, R.; Neal, L.; Palacios-Peña, L.; Savage, N.; Schaap, M.; et al. Evaluating cloud properties in an ensemble of regional online coupled models against satellite observations. *Atmos. Chem. Phys.* **2018**, *18*, 15183–15199. [CrossRef]
21. Péré, J.C.; Bessagnet, B.; Mallet, M.; Waquet, F.; Chiapello, I.; Minvielle, F.; Pont, V.; Menut, L. Direct radiative effect of the Russian wildfires and its impact on air temperature and atmospheric dynamics during August 2010. *Atmos. Chem. Phys.* **2014**, *14*, 1999–2013. [CrossRef]
22. Nabat, P.; Somot, S.; Mallet, M.; Michou, M.; Sevault, F.; Driouech, F.; Meloni, D.; di Sarra, A.; Di Biagio, C.; Formenti, P.; et al. Dust aerosol radiative effects during summer 2012 simulated with a coupled regional aerosol-atmosphere-ocean model over the Mediterranean. *Atmos. Chem. Phys.* **2015**, *15*, 3303–3326. [CrossRef]
23. Kong, X.; Forkel, R.; Sokhi, R.S.; Suppan, P.; Baklanov, A.; Gauss, M.; Brunner, D.; Barò, R.; Balzarini, A.; Chemel, C.; et al. Analysis of meteorology-chemistry interactions during air pollution episodes using online coupled models within AQMEII phase-2. *Atmos. Environ.* **2015**, *115*, 527–540. [CrossRef]

24. Baró, R.; Lorente-Plazas, R.; Montávez, J.P.; Jiménez-Guerrero, P. Biomass burning aerosol impact on surface winds during the 2010 Russian heat wave. *Geophys. Res. Lett.* **2017**, *44*, 1088–1094. [CrossRef]
25. Skamarock, W.C.; Klemp, J.B.; Dudhia, J.; Gill, D.O.; Barker, D.M.; Wang, W.; Powers, J.G. *A Description of the Advanced Research WRF Version 3*; Technical Report, NCAR Tech. Note TN-475+STR; NCAR: Boulder, CO, USA, 2008. [CrossRef]
26. Grell, G.A.; Peckham, S.E.; Schmitz, R.; McKeen, S.A.; Frost, G.; Skamarock, W.C.; Eder, B. Fully coupled -online- chemistry within the WRF model. *Atmos. Environ.* **2005**, *39*, 6957–6975. [CrossRef]
27. Hersbach, H.; Peubey, C.; Simmons, A.; Berrisford, P.; Poli, P.; Dee, D. ERA-20CM: A twentieth-century atmospheric model ensemble. *Q. J. R. Meteorol. Soc.* **2015**, *141*, 2350–2375. [CrossRef]
28. Jacob, D.; Petersen, J.; Eggert, B.; Alias, A.; Christensen, O.B.; Bouwer, L.M.; Braun, A.; Colette, A.; Déqué, M.; Georgievski, G.; et al. EURO-CORDEX: New high-resolution climate change projections for European impact research. *Reg. Environ. Chang.* **2014**, *14*, 563–578. [CrossRef]
29. Emmons, L.K.; Walters, S.; Hess, P.G.; Lamarque, J.F.; Pfister, G.G.; Fillmore, D.; Granier, C.; Guenther, A.; Kinnison, D.; Laepple, T.; et al. Description and evaluation of the Model for Ozone and Related chemical Tracers, version 4 (MOZART-4). *Geosci. Model Dev.* **2010**, *3*, 43–67. [CrossRef]
30. Jerez, S.; López-Romero, J.; Turco, M.; Jiménez-Guerrero, P.; Vautard, R.; Montávez, J. Impact of evolving greenhouse gas forcing on the warming signal in regional climate model experiments. *Nat. Commun.* **2018**, *9*, 1304. [CrossRef]
31. Lin, Y.L.; Farley, R.D.; Orville, H.D. Bulk Parameterization of the Snow Field in a Cloud Model. *J. Clim. Appl. Meteorol.* **1983**, *22*, 1065–1092. [CrossRef]
32. Tewari, M.; Chen, F.; Wang, W.; Dudhia, J.; LeMone, M.A.; Mitchell, K.; Ek, M.; Gayno, G.; Wegiel, J.; Cuenca, R.H. Implementation and verification of the unified NOAH land surface model in the WRF model. In Proceedings of the 20th Conference on Weather Analysis and Forecasting/16th Conference on Numerical Weather Prediction, Seattle, WA, USA, 12–16 January 2004; pp. 11–15.
33. Iacono, M.J.; Delamere, J.S.; Mlawer, E.J.; Shephard, M.W.; Clough, S.A.; Collins, W.D. Radiative forcing by long-lived greenhouse gases: Calculations with the AER radiative transfer models. *J. Geophys. Res. Atmos.* **2008**, *113*. [CrossRef]
34. Grell, G.A. Prognostic Evaluation of Assumptions Used by Cumulus Parameterizations. *Mon. Weather. Rev.* **1993**, *121*, 764–787. [CrossRef]
35. Grell, G.A.; Dévényi, D. A generalized approach to parameterizing convection combining ensemble and data assimilation techniques. *Geophys. Res. Lett.* **2002**, *29*, 38–1–38–4. [CrossRef]
36. Hong, S.Y.; Noh, Y.; Dudhia, J. A New Vertical Diffusion Package with an Explicit Treatment of Entrainment Processes. *Mon. Weather. Rev.* **2006**, *134*, 2318–2341. [CrossRef]
37. Lamarque, J.F.; Bond, T.C.; Eyring, V.; Granier, C.; Heil, A.; Klimont, Z.; Lee, D.; Liousse, C.; Mieville, A.; Owen, B.; et al. Historical (1850–2000) gridded anthropogenic and biomass burning emissions of reactive gases and aerosols: Methodology and application. *Atmos. Chem. Phys.* **2010**, *10*, 7017–7039. [CrossRef]
38. Jiménez-Guerrero, P.; Jerez, S.; Montávez, J.P.; Trigo, R.M. Uncertainties in future ozone and PM10 projections over Europe from a regional climate multiphysics ensemble. *Geophys. Res. Lett.* **2013**, *40*, 5764–5769. [CrossRef]
39. Tarín-Carrasco, P.; Morales-Suárez-Varela, M.; Im, U.; Brandt, J.; Palacios-Peña, L.; Jiménez-Guerrero, P. Isolating the climate change impacts on air-pollution-related-pathologies over central and southern Europe—A modelling approach on cases and costs. *Atmos. Chem. Phys.* **2019**, *19*, 9385–9398. [CrossRef]
40. Giorgi, F.; Meleux, F. Modelling the regional effects of climate change on air quality. *C. R. Geosci.* **2007**, *339*, 721–733. [CrossRef]
41. Goudie, A.; Middleton, N. Saharan dust storms: Nature and consequences. *Earth-Sci. Rev.* **2001**, *56*, 179–204. [CrossRef]
42. Middleton, N.J.; Goudie, A.S. Saharan dust: Sources and trajectories. *Trans. Inst. Br. Geogr.* **2001**, *26*, 165–181. [CrossRef]
43. Goudie, A.S.; Middleton, N.J. *Desert Dust in the Global System*; Springer Science & Business Media: London, UK, 2006; p. 288. [CrossRef]
44. Ginoux, P.; Chin, M.; Tegen, I.; Prospero, J.M.; Holben, B.; Dubovik, O.; Lin, S.J. Sources and distributions of dust aerosols simulated with the GOCART model. *J. Geophys. Res. Atmos.* **2001**, *106*, 20255–20273. [CrossRef]

45. Ahmadov, R.; McKeen, S.A.; Robinson, A.L.; Bahreini, R.; Middlebrook, A.M.; de Gouw, J.A.; Meagher, J.; Hsie, E.Y.; Edgerton, E.; Shaw, S.; et al. A volatility basis set model for summertime secondary organic aerosols over the eastern United States in 2006. *J. Geophys. Res. Atmos.* **2012**, *117*. [CrossRef]
46. Fast, J.D.; Gustafson, W.I., Jr.; Easter, R.C.; Zaveri, R.A.; Barnard, J.C.; Chapman, E.G.; Grell, G.A.; Peckham, S.E. Evolution of ozone, particulates, and aerosol direct radiative forcing in the vicinity of Houston using a fully coupled meteorology-chemistry-aerosol model. *J. Geophys. Res. Atmos.* **2006**, *111*. [CrossRef]
47. Guenther, A.; Karl, T.; Harley, P.; Wiedinmyer, C.; Palmer, P.I.; Geron, C. Estimates of global terrestrial isoprene emissions using MEGAN (Model of Emissions of Gases and Aerosols from Nature). *Atmos. Chem. Phys.* **2006**, *6*, 3181–3210. [CrossRef]
48. Malm, W.C.; Sisler, J.F.; Huffman, D.; Eldred, R.A.; Cahill, T.A. Spatial and seasonal trends in particle concentration and optical extinction in the United States. *J. Geophys. Res. Atmos.* **1994**, *99*, 1347–1370. [CrossRef]
49. Binkowski, F.S.; Roselle, S.J. Models-3 Community Multiscale Air Quality (CMAQ) model aerosol component 1. Model description. *J. Geophys. Res. Atmos.* **2003**, *108*. [CrossRef]
50. Jiménez-Guerrero, P.; Jorba, O.; Pay, M.T.; Montávez, J.P.; Jerez, S.; Gómez-Navarro, J.J.; Baldasano, J.M. Comparison of two different sea-salt aerosol schemes as implemented in air quality models applied to the Mediterranean Basin. *Atmos. Chem. Phys.* **2011**, *11*, 4833–4850. [CrossRef]
51. Basart, S.; Pay Pérez, M.T.; Jorba Casellas, O.; Pérez García-Pando, C.; Jiménez Guerrero, P.; Schulz, M.; Baldasano Recio, J.M. Aerosols in the CALIOPE air quality modelling system: Evaluation and analysis of PM levels, optical depths and chemical composition over Europe. *Atmos. Chem. Phys.* **2012**, *12*, 3363–3392. [CrossRef]
52. Chapman, E.G.; Gustafson, W.I., Jr.; Easter, R.C.; Barnard, J.C.; Ghan, S.J.; Pekour, M.S.; Fast, J.D. Coupling aerosol-cloud-radiative processes in the WRF-Chem model: Investigating the radiative impact of elevated point sources. *Atmos. Chem. Phys.* **2009**, *9*, 945–964. [CrossRef]
53. Rutledge, S.A.; Hobbs, P.V. The Mesoscale and Microscale Structure and Organization of Clouds and Precipitation in Midlatitude Cyclones. XII: A Diagnostic Modeling Study of Precipitation Development in Narrow Cold-Frontal Rainbands. *J. Atmos. Sci.* **1984**, *41*, 2949–2972. [CrossRef]
54. Tao, W.K.; Simpson, J.; McCumber, M. An Ice-Water Saturation Adjustment. *Mon. Weather. Rev.* **1989**, *117*, 231–235. [CrossRef]
55. Mitchell, D.L.; Rasch, P.; Ivanova, D.; McFarquhar, G.; Nousiainen, T. Impact of small ice crystal assumptions on ice sedimentation rates in cirrus clouds and GCM simulations. *Geophys. Res. Lett.* **2008**, *35*, L09806. [CrossRef]
56. Li, G.; Wang, Y.; Zhang, R. Implementation of a two-moment bulk microphysics scheme to the WRF model to investigate aerosol-cloud interaction. *J. Geophys. Res. Atmos.* **2008**, *113*, D15211. [CrossRef]
57. Ghan, S.J.; Leung, L.R.; Easter, R.C.; Abdul-Razzak, H. Prediction of cloud droplet number in a general circulation model. *J. Geophys. Res. Atmos.* **1997**, *102*, 21777–21794. [CrossRef]
58. Liu, Y.; Daum, P.H.; McGraw, R.L. Size truncation effect, threshold behavior, and a new type of autoconversion parameterization. *Geophys. Res. Lett.* **2005**, *32*, L11811. [CrossRef]
59. Inness, A.; Ades, M.; Agustí-Panareda, A.; Barré, J.; Benedictow, A.; Blechschmidt, A.M.; Dominguez, J.J.; Engelen, R.; Eskes, H.; Flemming, J.; et al. The CAMS reanalysis of atmospheric composition. *Atmos. Chem. Phys.* **2019**, *19*, 3515–3556 [CrossRef]
60. Huijnen, V.; Pozzer, A.; Arteta, J.; Brasseur, G.; Bouarar, I.; Chabrillat, S.; Christophe, Y.; Doumbia, T.; Flemming, J.; Guth, J.; et al. Quantifying uncertainties due to chemistry modelling—Evaluation of tropospheric composition simulations in the CAMS model (cycle 43R1). *Geosci. Model Dev.* **2019**, *12*, 1725–1752. [CrossRef]
61. Holben, B.; Eck, T.; Slutsker, I.; Tanré, D.; Buis, J.; Setzer, A.; Vermote, E.; Reagan, J.; Kaufman, Y.; Nakajima, T.; et al. AERONET—A Federated Instrument Network and Data Archive for Aerosol Characterization. *Remote Sens. Environ.* **1998**, *66*, 1–16. [CrossRef]
62. Haylock, M.R.; Hofstra, N.; Klein Tank, A.M.G.; Klok, E.J.; Jones, P.D.; New, M. A European daily high-resolution gridded data set of surface temperature and precipitation for 1950–2006. *J. Geophys. Res. Atmos.* **2008**, *113*, D20119. [CrossRef]

63. Wyant, M.C.; Bretherton, C.S.; Wood, R.; Carmichael, G.R.; Clarke, A.; Fast, J.; George, R.; Gustafson, W.I., Jr.; Hannay, C.; Lauer, A.; et al. Global and regional modeling of clouds and aerosols in the marine boundary layer during VOCALS: The VOCA intercomparison. *Atmos. Chem. Phys.* **2015**, *15*, 153–172. [CrossRef]
64. Stengel, M.; Stapelberg, S.; Sus, O.; Schlundt, C.; Poulsen, C.; Thomas, G.; Christensen, M.; Carbajal Henken, C.; Preusker, R.; Fischer, J.; et al. Cloud property datasets retrieved from AVHRR, MODIS, AATSR and MERIS in the framework of the Cloud_cci project. *Earth Syst. Sci. Data* **2017**, *9*, 881–904. [CrossRef]
65. Morrison, H.; Thompson, G.; Tatarskii, V. Impact of Cloud Microphysics on the Development of Trailing Stratiform Precipitation in a Simulated Squall Line: Comparison of One- and Two-Moment Schemes. *Mon. Weather. Rev.* **2009**, *137*, 991–1007. [CrossRef]
66. Webb, L.; Watterson, I.; Bhend, J.; Whetton, P.; Barlow, E. Global climate analogues for winegrowing regions in future periods: Projections of temperature and precipitation. *Aust. J. Grape Wine Res.* **2013**, *19*, 331–341. [CrossRef]
67. Schaap, M.; Timmermans, R.; Koelemeijer, R.; de Leeuw, G.; Builtjes, P. Evaluation of MODIS aerosol optical thickness over Europe using sun photometer observations. *Atmos. Environ.* **2008**, *42*, 2187–2197. [CrossRef]
68. Querol, X.; Pey, J.; Pandolfi, M.; Alastuey, A.; Cusack, M.; Pérez, N.; Moreno, T.; Viana, M.; Mihalopoulos, N.; Kallos, G.; et al. African dust contributions to mean ambient PM10 mass-levels across the Mediterranean Basin. *Atmos. Environ.* **2009**, *43*, 4266–4277. [CrossRef]
69. Palacios-Peña, L.; Baró, R.; Guerrero-Rascado, J.L.; Alados-Arboledas, L.; Brunner, D.; Jiménez-Guerrero, P. Evaluating the representation of aerosol optical properties using an online coupled model over the Iberian Peninsula. *Atmos. Chem. Phys.* **2017**, *17*, 277–296. [CrossRef]
70. Pozzer, A.; de Meij, A.; Yoon, J.; Tost, H.; Georgoulias, A.K.; Astitha, M. AOD trends during 2001–2010 from observations and model simulations. *Atmos. Chem. Phys.* **2015**, *15*, 5521–5535. [CrossRef]
71. Matthias, V. The aerosol distribution in Europe derived with the Community Multiscale Air Quality (CMAQ) model: Comparison to near surface in situ and sunphotometer measurements. *Atmos. Chem. Phys.* **2008**, *8*, 5077–5097. [CrossRef]
72. Pay, M.T.; Jiménez-Guerrero, P.; Baldasano, J.M. Assessing sensitivity regimes of secondary inorganic aerosol formation in Europe with the CALIOPE-EU modeling system. *Atmos. Environ.* **2012**, *51*, 146–164. [CrossRef]
73. Prijith, S.; Aloysius, M.; Mohan, M. Relationship between wind speed and sea salt aerosol production: A new approach. *J. Atmos. Sol.-Terr. Phys.* **2014**, *108*, 34–40. [CrossRef]
74. Li, S.; Wang, T.; Xie, M.; Han, Y.; Zhuang, B. Observed aerosol optical depth and angstrom exponent in urban area of Nanjing, China. *Atmos. Environ.* **2015**, *123*, 350–356. [CrossRef]
75. Wang, K.; Yahya, K.; Zhang, Y.; Hogrefe, C.; Pouliot, G.; Knote, C.; Hodzic, A.; Jose, R.S.; Perez, J.L.; Jiménez-Guerrero, P.; et al. A multi-model assessment for the 2006 and 2010 simulations under the Air Quality Model Evaluation International Initiative (AQMEII) Phase 2 over North America: Part II. Evaluation of column variable predictions using satellite data. *Atmos. Environ.* **2015**, *115*, 587–603. [CrossRef]
76. Lapina, K.; Heald, C.L.; Spracklen, D.V.; Arnold, S.R.; Allan, J.D.; Coe, H.; McFiggans, G.; Zorn, S.R.; Drewnick, F.; Bates, T.S.; et al. Investigating organic aerosol loading in the remote marine environment. *Atmos. Chem. Phys.* **2011**, *11*, 8847–8860. [CrossRef]
77. Balzarini, A.; Pirovano, G.; Honzak, L.; Žabkar, R.; Curci, G.; Forkel, R.; Hirtl, M.; José, R.S.; Tuccella, P.; Grell, G. WRF-Chem model sensitivity to chemical mechanisms choice in reconstructing aerosol optical properties. *Atmos. Environ.* **2015**, *115*, 604–619. [CrossRef]
78. Pérez, C.; Nickovic, S.; Pejanovic, G.; Baldasano, J.M.; Ozsoy, E. Interactive dust-radiation modeling: A step to improve weather forecasts. *J. Geophys. Res. Atmos.* **2006**, *111*, D16. [CrossRef]
79. Pérez, C.; Haustein, K.; Janjic, Z.; Jorba, O.; Huneeus, N.; Baldasano, J.M.; Black, T.; Basart, S.; Nickovic, S.; Miller, R.L.; et al. Atmospheric dust modeling from meso to global scales with the online NMMB/BSC-Dust model—Part 1: Model description, annual simulations and evaluation. *Atmos. Chem. Phys.* **2011**, *11*, 13001–13027. [CrossRef]